Percept-related EEG classification using machine learning approach and features of functional brain connectivity

Cite as: Chaos **29**, 093110 (2019); https://doi.org/10.1063/1.5113844
Submitted: 08 June 2019 . Accepted: 08 August 2019 . Published Online: 09 September 2019

Alexander E. Hramov, Vladimir Maksimenko, Alexey Koronovskii, Anastasiya E. Runnova, Maxim Zhuravlev, Alexander N. Pisarchik, and Jürgen Kurths

Percept-related EEG classification using machine learning approach and features of functional brain connectivity

Cite as: Chaos **29**, 093110 (2019); doi: 10.1063/1.5113844
Submitted: 8 June 2019 · Accepted: 8 August 2019 ·
Published Online: 9 September 2019

View Online Export Citation CrossMark

Alexander E. Hramov,[1,a)] Vladimir Maksimenko,[1] Alexey Koronovskii,[2] Anastasiya E. Runnova,[1] Maxim Zhuravlev,[1] Alexander N. Pisarchik,[1,3] and Jürgen Kurths[4,5,6]

AFFILIATIONS

[1]Neuroscience and Cognitive Technology Laboratory, Center for Technologies in Robotics and Mechatronics Components, Innopolis University, 420500 Innopolis, The Republic of Tatarstan, Russia
[2]Faculty of Nonlinear Processes, Saratov State University, 410012 Saratov, Russia
[3]Center for Biomedical Technology, Technical University of Madrid, 28223 Pozuelo de Alarcon, Madrid, Spain
[4]Potsdam Institute for Climate Impact Research, 14473 Potsdam, Germany
[5]Department of Physics, Humboldt University, 12489 Berlin, Germany
[6]Biology Department, Saratov State University, 410012, Saratov, Russia

Note: This paper is part of the Focus Issue, "When Machine Learning Meets Complex Systems: Networks, Chaos and Nonlinear Dynamics."

[a)]**Electronic mail:** a.hramov@innopolis.ru

ABSTRACT

Machine learning is a promising approach for electroencephalographic (EEG) trials classification. Its efficiency is largely determined by the feature extraction and selection techniques reducing the dimensionality of input data. Dimensionality reduction is usually implemented via the mathematical approaches (e.g., principal component analysis, linear discriminant analysis, etc.) regardless of the origin of analyzed data. We hypothesize that since EEG features are determined by certain neurophysiological processes, they should have distinctive characteristics in spatiotemporal domain. If so, it is possible to specify the set of EEG principal features based on the prior knowledge about underlying neurophysiological processes. To test this hypothesis, we consider the classification of EEG trials related to the perception of ambiguous visual stimuli. We observe that EEG features, underlying the different ambiguous stimuli interpretations, are defined by the network properties of neuronal activity. Having analyzed functional neural interactions, we specify the brain area in which neural network architecture exhibits differences for different classes of EEG trials. We optimize the feedforward multilayer perceptron and develop a strategy for the training set selection to maximize the classification accuracy, being 85% when all channels are used. The revealed localization of the percept-related features allows about 95% accuracy, when the number of channels is reduced up to 90%. Obtained results can be used for classification of EEG trials associated with more complex cognitive tasks. Taking into account that cognitive activity is subserved by a distributed functional cortical network, its topological properties have to be considered when selecting optimal features for EEG trial classification.

The optimization problem is very important for brain-computer interfaces (BCIs) based on the electroencephalographic (EEG) trial classification with the help of machine learning methods. The accuracy of machine learning approaches to EEG trial classification depends on the proper selection of the principal EEG features. At first glance, this selection can be performed by determining a featured brain area and frequency band, based on the event-related potential (ERP) or time-frequency EEG analysis. However, even for motor activity, for which the spatial and frequency domains are relatively well defined, the restricting analysis to a few predefined trials sometimes leads to worsening of the classification accuracy. For the more complex brain activity, e.g., perceptual decision-making, EEG features selection is a more sophisticated problem because this activity is performed by functional neural interactions within a distributed cortical network. However, this issue can be addressed by analyzing the properties of functional interactions between EEG channels. With this goal in mind, we classify EEG trials associated with different

interpretations of ambiguous visual stimuli. Analysis of spatiotemporal and time-frequency features does not reveal differences between the classes of trials. At the same time, functional connectivity analysis shows that differences are hidden in the neural interactions within the occipital and parietal cortices. The revealed localization of the percept-related features allows about 95% accuracy when the number of EEG channels is reduced up to 90%.

I. INTRODUCTION

Machine learning approaches are widely applied for analysis and prediction of nonlinear systems dynamics.[1,2] In particular, a reservoir-computing-based method is used for data-driven model-free estimation of the Lyapunov exponents,[3] and for attractor reconstruction[4] of chaotic processes, echo state networks (ESNs) are applied for the detection of generalized synchronization.[5] In this context, an exciting challenge of machine learning is its ability to extract particular features from a single trial, thus providing the possibility to detect and classify different patterns in electroencephalographic (EEG) data in real time. A variety of different machine learning based methods have been developed for the analysis of neurophysiological signals. Among them, one can highlight the support-vector machine (SVM) often used for EEG data processing in order to extract movement-related features.[6] In particular, artificial neural networks (ANNs) based on nonlinear models of neural units inspired by biological interconnected neurons are widely used in computational biology for classification of EEG trials.[7] Multilayer perceptron (MLP) detects the nonlinear process of decision-making in the human brain.[8] Specifically, a type of ANN, the convolutional neural networks (CNNs) are known to be a powerful tool for pattern recognition in different data, including EEG recordings.[9]

Along with the promising possibility of machine learning approaches to classify different EEG trials, recent studies provide insight into spatial characteristics of EEG patterns associated with real and imagery movements,[10] visual perception,[11] and the development of brain-computer interfaces (BCIs).[12–14] In the BCI research, the tasks of multichannel EEG classification with the help of machine learning often face the optimization problem.[15] All possible features of a multichannel EEG result in an extremely large phase-space dimension that has to be processed by the classifier. This is a critical issue for BCI, where calculations should be performed in real time by portable computers, where the calculation performance is of extreme importance.

In neuroscience, the optimization problem can be solved by using several techniques. Common methods of dimensional reduction include principal component analysis (PCA) and linear discriminant analysis (LDA), where the original features are mathematically projected onto a lower-dimensional phase space. In particular, Alpert *et al.*[16] used PCA to reduce the phase-space dimension, while classifying percept-related EEG trials. Recently, a similar approach was also applied for classification of data sets from a postural control protocol[17] and sleep-related neurophysiological data.[18] Furthermore, LDA was used for classification of motor-related EEGs[19] and EEG features associated with pathological activity, such as dementia and Alzheimer disease.[20] There are also optimization approaches based on genetic algorithms (GAs) allowing a feature set, which yields a high classification precision. These methods have been recently used for classification of biological signals, such as electrocardiogram (ECG),[21] EEG related to different types of imaginary movements,[22] and pathological activity including epileptic seizures.[23]

The approaches described above do not take into account the origin of the analyzed data. On the contrary, we hypothesize that since EEG features are determined by certain neurophysiological processes, they should have distinctive characteristics either in time-frequency or spatiotemporal domains. If so, it is possible to specify the set of principal spatiotemporal and time-frequency EEG features based on the prior knowledge about underlying neurophysiological processes. With this in mind, in the recent work,[10] we used MLP for classification of motor-related EEG trials and related the choice of the MLP input features with the spatiotemporal and time-frequency EEG structure. Namely, EEG analysis revealed spectral and spatial properties associated with the pronounced differences in different classes of EEG trials. Using these particular properties allowed to reduce the number of input signals from 31 to 8 and to achieve to $90 \pm 5\%$ classification accuracy.

While the correlation between MLP classification performance and spatiotemporal and time-frequency EEG properties has been reported for the motor-related EEG, this issue remains unresolved for cognitive tasks. One can expect that motor activity in the brain is subserved by a generation of well-defined rhythms of neural activity in the well-established areas (e.g., mu-rhythm in the motor cortex and theta-rhythm in the frontal cortex). For cognitive activity, the spatial features cannot be easily specified since it is implemented via the activation of spatially distributed cortical networks.[24] At the same time, we suppose that in the case of cognitive activity, EEG feature selection can be based on the topological properties of the cortical network.

In order to test this hypothesis, in the present work, we analyze the brain activity associated with the processing the ambiguous stimuli (Necker cubes). According to Kornmeier *et al.*,[25] the Necker cube interpretation can be considered as a cognitive decision process. Recently, we have shown that multilayer perceptron (MLP) is able to classify EEG trials, associated with different Necker cube interpretations.[11] In that work, we used EEG sensors covering the whole head surface; therefore, it was unknown whether the stimulus-related features of neuronal activity were distributed over large cortical areas or they belonged to a particular area. Unlike motor-related activity,[10,26] analysis of the spatiotemporal and time-frequency EEG features did not reveal differences in the classified classes of EEG trials.[11]

According to this, the main purpose of this current work is to relate the optimal EEG features for MLP input with the network properties of neuronal activity underlying ambiguous stimuli processing. With this in mind, we demonstrate that the EEG features, underlying the different ambiguous stimuli interpretations, are defined by the network properties of neuronal activity. Having analyzed functional neural interactions, we specify the brain area in which functional network architecture exhibits differences for different classes of EEG trials. Using the EEG signal from this particular brain area allows reducing the number of EEG channels from 19 to 2 and achieves 95% classification accuracy.

II. MATERIALS AND METHODS

A. Subjects

Twenty-five subjects participated in the experiments (17 males and 8 females, of the mean age of 24 years with a standard deviation of 5 years. All subjects were students and staff members of the Yury Gagarin State Technical University of Saratov, without any previous training in the task. All subjects had normal or corrected-to-normal vision, with no neurological diseases, free from psychoactive medications at the time of the experiment. The subjects were unpaid volunteers. All participants have provided an informed written consent before their participation in the experiment. The experimental study was carried out according to ethical standards[27] and approved by the Ethics Committee of the Innopolis University.

B. Bistable visual stimuli and experimental setup

Subjects were facing a display screen on which ambiguous images were displayed as visual stimuli [Fig. 1(a)], specifically, the Necker cube.[28,29] Necker cube images are presented in Fig. 1(b). One can see that depending on the intensity of inner ribs, Necker cube can be treated as oriented in two different ways—left- or right-oriented. The contrast of the three inner lines centered in the left middle corner is used as the control parameter $g \in [0, 1]$. The values $g = 1$ and $g = 0$ correspond, respectively, to 0 (black) and 255 (white) pixels' luminance of these three ribs. On the other hand, the contrast of the three inner ribs centered in the right middle corner was defined as $(1 - g)$. Finally, the normalized contrast of the six outer ribs was constant and equal to 1. During our experiment, $M = 7$ cube images with different wireframe contrasts, i.e., different values of the control parameter: $g = 0.15$ (practically fully left-oriented cubes), 0.3, 0.4, 0.5, 0.6, 0.7, and 0.85 (practically fully right-oriented cubes) were repeatedly presented to subjects in a random sequence, as shown in Figs. 1(b) and 1(c). All subjects were previously informed about two possible orientations of the Necker cube and able to see them.

Similarly to Ref. 11, stimuli were demonstrated on 24 in. (1920 × 1080 pixels) LCD monitor with a refresh rate of 60 Hz. Each Necker cube image with black and gray ribs was displayed in the middle of a computer screen on a white background. The subjects were sat at a 70–80 cm distance from the monitor with an approximately 0.25-rad visual angle.

C. Experimental protocol

In order to avoid possible adaptation and personal habituation in solving the task, every subject took part in only one experimental session. To exclude the influence of the real or imaginary motor reaction after the image presentation and to automatize the experimental procedure, we propose the following experimental design. Before the experiment, every subject was instructed how they should indicate his/her decision about cube orientation. There were two possible ways to do this. In the first series of the experiments, they must press either the left or the right key on the control panel according to their first visual impression, whereas in the second series, they must answer one of the two following questions randomly appearing on the screen:

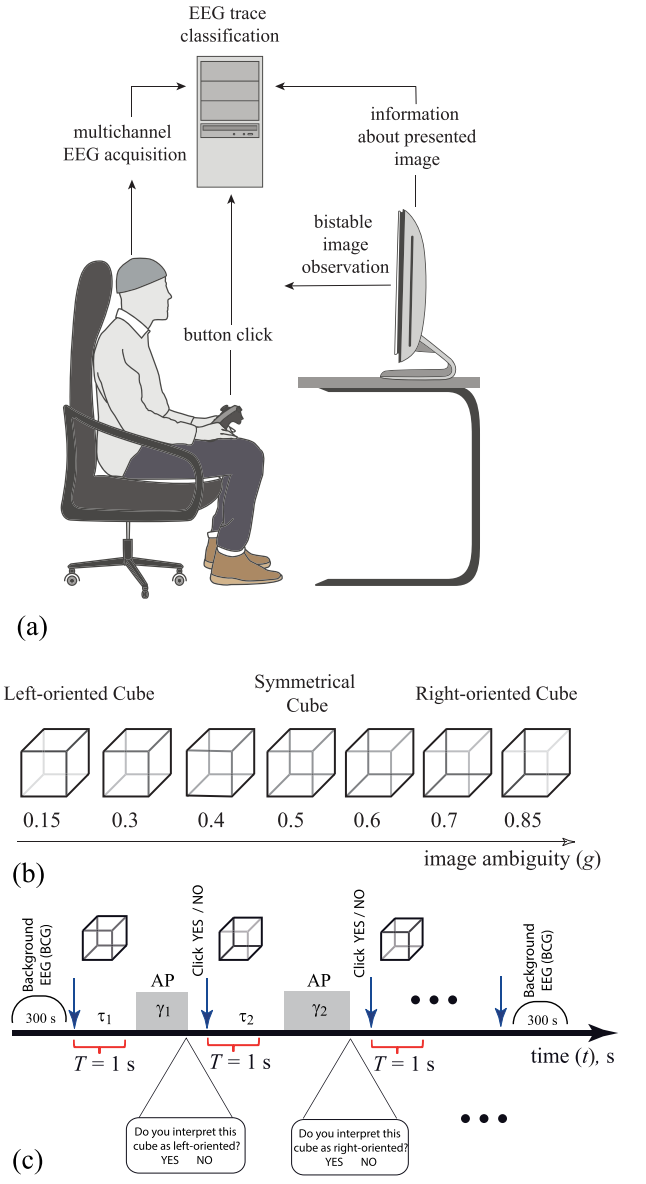

FIG. 1. (a) Experimental setup. (b) Necker cubes with different degrees of ambiguity g: $g = 0.15$ corresponds to left-oriented cube, $g = 0.85$ to right-oriented cube, and $g \sim 0.5$ to symmetrical cube. (c) Experimental session: the arrows show starting points of each presentation; time intervals $\tau_1, \tau_2, \ldots, \tau_N$ ($\tau = 0.8$–1.3 s, $N = 400$) correspond to the duration of each image presentation; time intervals $\gamma_1, \gamma_2, \ldots, \gamma_N$ ($\gamma = 2.0$–3.0 s, $N = 350$) indicate epochs for presentation of abstract pictures (APs). The red brackets below the time axis indicate $T = 1$ s periods of time during which the EEG data were taken for the ANN analysis.

(1) Do you interpret this cube as left-oriented? (If YES, then press the right key, otherwise press the left key).
(2) Do you interpret the cube as right-oriented? (If YES, then press the right key, otherwise press the left key).

The right key was associated with a positive answer, while the left key with a negative answer. Thus, the subject did not know in advance which key (left or right) he/she will press until the question (1) or (2) appears on the screen. This fact made his/her reaction independent of the imaginary movement associated with the preparation to press either left or right key during perception.

According to works,[30–32] in order to fix the first impression and avoid switches between two possible percepts, the image exhibition was limited to $\tau = 1.0$–1.4 s. In addition, to divert attention and make the perception of the next Necker cube image independent of the previous one, abstract pictures were exhibited for about $\eta = 2.0$–4.0 s between subsequent demonstrations of different Necker cube images. The duration of stimuli presentations τ_i and the intervals between stimuli η_i were randomly chosen from the defined above time intervals.

In order to diminish the effect of a persistent visual perception between subsequent presentations of ambiguous images,[33,34] Necker cubes with different parameter values g were presented in a random sequence, and the values of η_i were chosen to be sufficiently large.

After the abstract picture presentation, the questions (1) or (2) appeared on the screen, and the subject pressed the corresponding button on the keypad to indicate his/her first visual impression on the Necker cube orientation. After the click was done, the next Necker cube image with randomly selected parameter g was shown.

The schematic illustration of the experimental protocol is presented in Fig. 1(c). The following protocol was used in each of the runs:

1. 300-s background EEG activity (BCG) recording when the subject was in a relaxed state [Fig. 1(c)].
2. 40-min main part of the experiment, which includes demonstrating $M = 300$ Necker cubes with different values of the control parameter g. This part consists of six steps.
    1. The visual stimuli (the Necker cubes with a randomly chosen contrast parameter g) were displayed on the screen for a randomly chosen time interval τ_i between 1.0 s and 1.4 s.
    2. After observing the stimulus on the screen, the subject analyzed and memorized his/her first visual impression on the cube's orientation as left or right.
    3. Then, abstract pictures (APs) were exhibited for a randomly chosen time interval $\gamma_i \in [2, 3]$ s to divert attention and make the perception of the next image independent of the previous one.
    4. Next, the randomly selected question from two possible variants: (1) Do you interpret this cube as left-oriented? and (2) Do you interpret the cube as right-oriented? appeared on the screen.
    5. To answer this question, the subject pressed either left or right button, depending on his/her impression on the cube's orientation.
    6. Immediately after pressing the button, a next visual stimulus (the Necker cube with randomly chosen contrast parameter g) was displayed on the screen and the process was repeated $N = 400$ times.
3. 300-s background EEG activity (BCG) recording.

Experimental protocol, including the time markers of the stimuli presentations, subject's response and parameter g, were automatically recorded for further analysis of EEG data.

D. EEG registration and preprocessing

Multichannel EEG was recorded at a 250-Hz sampling rate from $P = 19$ electrodes with two reference electrodes placed at standard positions of the 10–20 international system.[35]

Similarly to Ref. 11, we used electroencephalograph "Encephalan–EEGR–19/26" (Taganrog, Russian Federation) with multiple EEG channels and two-button input device (keypad) and performed all necessary procedures to increase the conductivity of the skin and reduce its resistance. Machine learning algorithms were implemented with MATLAB.

Before loading data to ANN, large amplitude artifacts caused by eye blinks and movements in the frontal cortex were removed from EEG data with the help of the original software, using EOG and Gram-Schmidt orthogonalization procedures (for details, see Ref. 11).

Single 1-s trials corresponding to $N_T = 250$ samples were extracted from all EEG data sets of every subject. These single trials were $s_{pn}(t)$ ($p = 1, \ldots, P$, $n = 1, \ldots, N_T$) (P being the number of EEG channels). Each trial started at the beginning of the presentation of each Necker cube with the contrast parameter g, and ended 1 s after the stimulus onset [see Fig. 1(c)]. All trials were sorted in two classes (left- or right-oriented interpretation of bistable stimulus) in accordance with the key (left or right click) choice on the keypad. Finally,

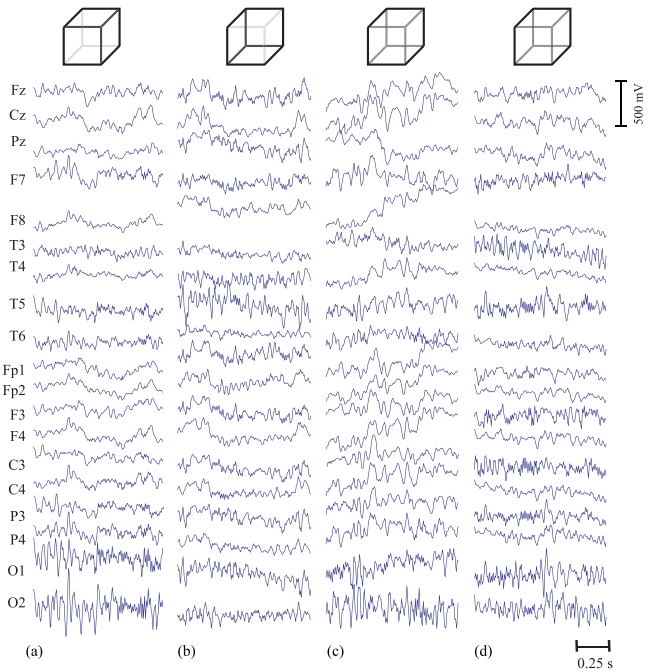

FIG. 2. Typical EEG trials after their preprocessing, corresponding to different Necker cube interpretations, recorded during $T = 1$ s after image presentation.

the trials extracted from each EEG electrode for each stimulus were scaled to the [0, 1] interval.

Figure 2 demonstrates typical EEG trials registered from all 19 electrodes and preprocessed with the procedure described above. Trials are shown for the cases of well-pronounced left- [$g = 0.15$, Fig. 2(a)] and right-oriented [$g = 0.85$, Fig. 2(b)] cubes, and left- [Fig. 2(c)] and right-oriented [Fig. 2(d)] interpretations of the symmetric cube with maximum ambiguity ($g = 0.5$).

Figure 2 demonstrates typical EEG trials of one of the subjects recorded from all 19 electrodes after the preprocessing procedure. These EEG traces of $T = 1$ s duration (250 samples) were registered just after the Necker cube presentation. The sets of the EEG traces corresponding to different interpretations of the Necker cube are shown for the cases of well-pronounced left- [$g = 0.15$, Fig. 2(a)] and right-oriented [$g = 0.85$, Fig. 2(b)] cubes, and left- [Fig. 2(c)] and right-oriented [Fig. 2(d)] interpretations of the symmetric cube with maximum ambiguity ($g = 0.5$). The trials of 25 subjects were used as initial databases to extract features from the time series using the ANN time domain technique.

E. ANN architecture and classification algorithm

We use a deep learning method based on ANN for single-trial EEG classification, where the nth single-trial data are represented by the spatiotemporal activity matrix S_n of size $D \times N_T$, containing raw event-related signals $s_p(t)$ ($p = 1, \ldots, D$) recorded from D EEG channels at all $N_T = 250$ time points, immediately after the image presentation. The value

$$Y_n = f(S_n) = \begin{cases} 1, & \text{left-oriented cube} \\ & \text{interpretation,} \\ 0, & \text{right-oriented one} \end{cases} \quad (1)$$

stands for the binary decision of the classification algorithm for the single-trial spatiotemporal EEG data matrix S_n corresponding to the left-/right-oriented Necker cube interpretation by the subject.

There are many different types of ANN, which are known to be a promising tool for pattern recognition and classification.[7,9,36] Similarly to our recent work,[11] in this study, we use a multilayer perceptron (MLP) characterized by signals traveling from left to right on a layer-by-layer basis (feedforward network).[36] MLP is an universal and popular class of ANN, widely used for a broad range of applications including classification.[37–42] In our case, the classification problem is the recognition of two different multistable brain states corresponding to the perception of ambiguous Necker cubes as left- or right-oriented. MLP is an universal and popular class of ANN, widely used for a broad range of applications including classification.[37–42] In our case, the classification problem is the recognition of two coexisting brain states corresponding to two different interpretations of the Necker cube orientation, either left or right.

Figure 3(a) shows the ANN architecture of MLP with two hidden layers. The first layer ("Input Layer—IL") contains D inputs equal to the number of EEG channels used for the analysis with the maximum of $D = P = 19$ corresponding to a complete set of EEG channels. The functional 1-s trial $s_p(t)$ (250-sample time series) was sent to the corresponding pth input from pth EEG channel, different for left or right cube interpretation. The signals from each input were enter to all nodes (artificial neurons) of the first hidden layer

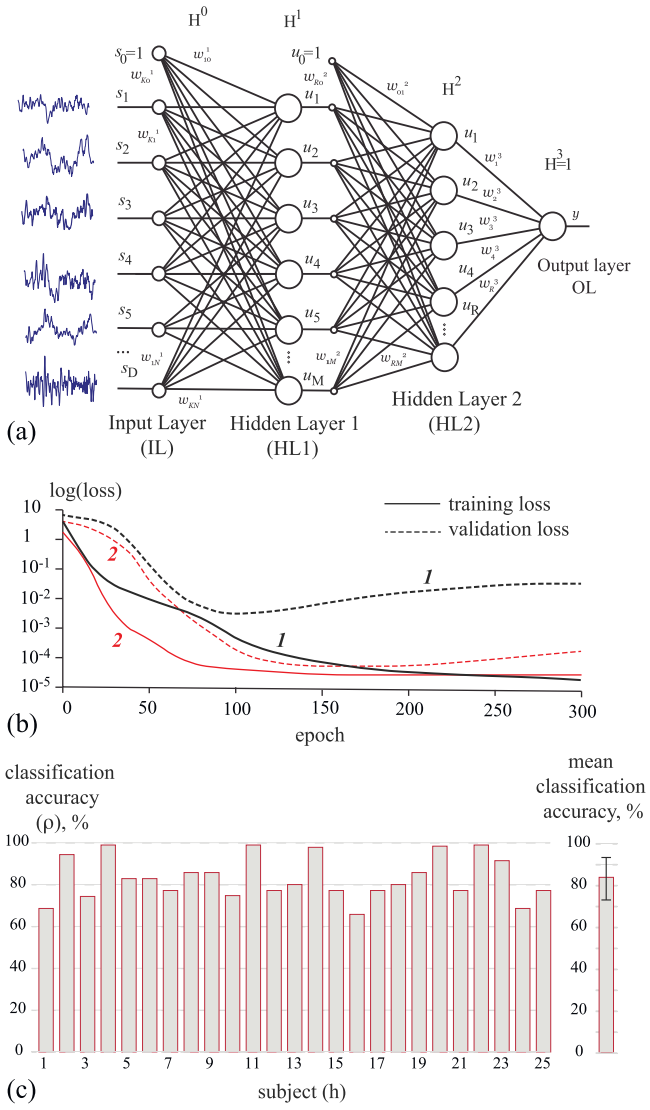

FIG. 3. (a) Multilayer perceptron (MLP) architecture with two hidden layers: IL ($l = 0$)—input layer, HL1, HL2—the first ($l = 1$) and second ($l = 2$) hidden layers, and OL—output layer ($l = 3$) . The number of inputs is $H^0 = D$, the numbers of nodes within the hidden layers are H^1 and H^2, and $s_0 = 1$ and $u_0 = 1$ are single constant inputs defined by the thresholds for neurons in the lth layer. (b) ANN training and validation loss curves for classification of EEG trials with all the channels (curves 1) and with only two O1 and O2 channels (curves 2). (c) Classification accuracy obtained for all 25 subjects when using all $D = P = 19$ EEG channels. The right panel represents the data averaged over all subjects under study.

("Hidden Layer 1—HL1") containing H_1 neurons. The resulting outputs of the first hidden layers were then sent to the second hidden layer ("Hidden Layer 2—HL2") with the same type of computational nodes. The number of nodes in the second hidden layer was equal to H_2. Finally, output layer (OL) includes one single neuron. Our task

was to recognize only two brain states corresponding to either left or right orientations. Therefore, it is convenient to consider a condition that the signal value from the output artificial neuron should be 0 or 1 [see Eq. (1), respectively].

The ANN evolution can be described by the following mathematical model:[43]

$$u_i^l(t) = F^l\left(\sum_{p=0}^{H^{l-1}} w_{pi}^l u_p^{l-1}(t)\right), \tag{2}$$

where H^l is the number of neurons in the lth layer (a layer with $l = 0$ is the input layer), $u_i^l(t)$ is the output signal of the ith neuron in the lth layer ($u_i^0(t)$ are signals from analyzed EEG channels), $\mathbf{W}^l = \{w_{pi}^l\}$ is the weight matrix of the lth layer in which dimension is $(H^{l-1} \times H^l)$, w_{pi}^l $(p = 0, \ldots, H^{l-1}, i = 1, \ldots, H^l)$ are the synaptic weights of input signals for the ith neuron in the lth layer. Similarly to the MLP, used in previous study,[11] neurons in the hidden layers ($l = 1, 2$) have nonlinear function of logistic activation ("sigmoid"), while the output neuron ($l = 3$) has linear activation function. We chose a "sigmoid" according to Ref. 44 as a common choice in the case of input data that takes real values and normalized in the range $[0, 1]$, and output lies also in the same range.

A class of recognized objects can be characterized by the mean squared value $\bar{y}$ of the signal coming from output neuron (i.e., $y(t_i) = u_1^3(t_i)$). For the left-oriented interpretation, $\bar{y} \geq 0.5$, whereas the right-oriented interpretation should give $\bar{y} < 0.5$. The binary decision of the classification algorithm for an nth EEG trial is defined as

$$Y_n = H(\bar{y} - 0.5), \tag{3}$$

where H is the Heaviside step function.

The unknown matrices $\mathbf{W}^l$ can be obtained during the learning process by minimizing the classification error criterion

$$\mu = \sqrt{\frac{1}{K}\sum_{k=1}^{K}\left(d_k - y_k\right)^2}, \tag{4}$$

where K is the total number of objects in the training set, y_k is the mean squared value of the output signal for the kth object, and d_k is a desired output value of y_k to teach MLP. In particular, $d_k = 1$ corresponds to the left-oriented cube and $d_k = 0$ to the right-oriented cube. The unknown ANN parameters are searched by using the Levenberg-Marquardt algorithm (LMA).[45] By differentiating the error criterion in Eq. (4) with respect to the unknown parameters, the LMA method gives better results in comparison with other optimization methods, but requires more computational time to determine the unknown parameters.

The method's classification performance is measured by the percentage of correct classification of single EEG trials interpreted as left-/right cube orientations, called "recognition accuracy" ρ (in percentages) of ambiguous images.

To estimate the ANN learning results, we repeated the training procedure many times (1000 learning cycles in total). As a consequence, we obtained 1000 ANNs with different parameters and different values of classification error μ, from which we chose the ANN with smallest classification error obtained with accuracy ρ as the best ANN for classification to be used for further analysis. The ANN learning process was individually implemented for each subject to obtain his/her optimal ANN architecture with highest classification accuracy. It should be noted that the ANNs were trained for each subjects separately, that is, we created a classifier of EEG trials for each subject. Earlier in Ref. 11, we demonstrated that there is the possibility of ANN training on the data set of one subject for classifying EEG trials of other subjects. However, in this case, the accuracy of the classification depends strongly on the subject's data set to train. At the same time, the classification accuracy in the case of ANN trained separately for each subject remains high for all the participants.

In order to find an optimal algorithm and the best configuration of the ANN architecture for brain states classification during ambiguous images perception, we systematically analyze the influence of a learning data set, the number H^l of artificial neurons in hidden layers, and a set of EEG channels to provide reasonable recognition accuracy ρ.

F. Wavelet coherence based functional brain connectivity

The interaction degree between cortical and thalamical EEG channels in different frequencies f was measured in $T = 1$ s time intervals, related to the Necker cube interpretation after stimulus presentation, using the wavelet coherence.[46] This approach is widely used for the analysis of links between neurophysiological signals.[47–49]

A continuous wavelet cross-spectrum is defined as

$$K_{l,m}(f, \Delta\tau) = \int_T W_l(f, \tau) W_m^*(f, \tau + \Delta\tau) d\tau, \tag{5}$$

where W_l and W_m are the continuous wavelet spectra $s_l(t)$ and $s_m(t)$ of EEG signals recorded from lth and mth EEG channels, respectively, given as

$$W_{l,m}(f, t) = \sqrt{f}\int_{-\infty}^{+\infty} s_{l,m}(t)\psi^*\left((t' - t)f\right) dt', \tag{6}$$

with mother Morlet wavelet[50]

$$\psi(\theta) = \frac{1}{\sqrt[4]{\pi}}\exp\left(\sqrt{-1}2\pi\theta\right)\exp\left(-\frac{\theta^2}{2}\right), \tag{7}$$

where $*$ denotes complex conjugation and $\Delta\tau$ is the delay time. The wavelet cross-spectrum allows the estimation of a change in the signal structure in time intervals separated by delay $\Delta\tau$.

Usually, the normalized wavelet cross-spectrum (wavelet coherence) is considered as

$$\gamma_{l,m}(f, \Delta\tau) = \frac{K_{l,m}(f, \Delta\tau)}{\sqrt{\langle E_l(f)\rangle \langle E_m(f)\rangle}}, \tag{8}$$

taking values in the interval $[0, 1]$. Here,

$$\langle E_{l,m}(f)\rangle = \frac{1}{T}\int_T W_{l,m}\, dt \tag{9}$$

are time averaged distributions of the wavelet energy over frequencies. Obviously, the greater the interaction degree between signals $s_l(t)$ and $s_m(t)$, the closer to 1 the wavelet coherence $\gamma_{l,m}$ can be interpreted as interaction strength.[51]

III. RESULTS

A. Spatiotemporal analysis

For the learning process, we created a training data set consisting of 70 single 1-s duration trials (250 samples) selected from EEG recordings obtained from each subject using the following strategies:

(i) We randomly selected 70 EEG trials corresponding to the Necker cubes with different contrast parameters $g = 0.15, 0.3, 0.4, 0.5, 0.6, 0.7, 0.85$.
(ii) We randomly selected $N = 10$ EEG trials corresponding to every value of the contrast parameter from $g = 0.15, 0.3, 0.4, 0.5, 0.6, 0.7, 0.85$.
(iii) We randomly selected 70 EEG trials corresponding to the Necker cubes with high ambiguity $g = 0.3, 0.4, 0.5, 0.6, 0.7$ only, i.e., excluding cubes with low ambiguity $g = 0.15, 0.85$.
(iv) We randomly selected 70 EEG trials corresponding to the Necker cubes with low ambiguity $g = 0.15, 0.85$ only, i.e., excluding cubes with high ambiguity.

For the validation process, we created a validation data set consisting of 70 single 1-s duration trials (250 samples) selected randomly from remaining EEG recordings obtained from each subject. To check the accuracy of classification, we utilized the remaining EEG trace, which we did not use for ANN training and validation, in particular, we tested 160 trials related to demonstration of the cubes with different ambiguities.

In order to analyze our classification algorithm, we first trained the ANN using all registered channels $D = P = H^0 = 19$ as input signals. We chose the number of neurons in the first hidden layer to be equal to the number of input channels, i.e., $H^1 = 19$ and the number of neurons in the second hidden layer to be equal to $H^2 = 5$, based on our previous analysis.[8,11] The training data set was formed for each individual using the first strategy (i) and included 70 EEG trials corresponding to every value of the contrast parameter g. We repeated the training procedure 1000 times and, as a consequence, we obtained the optimal set of ANN parameters

$$\Gamma_h = (\mathbf{W}_h^1, \mathbf{W}_h^2, \mathbf{W}_h^3) \tag{10}$$

($h = 1, \ldots, 25$ being the subject number) for classification of the brain states of subject h. Figure 3(b) shows the ANN performance, which is presented as the dependences of the training (black solid curve 1) and validation (black dotted curve 1) classification loss on the number of learning epochs in the case of optimal ANN Γ_h (10) for subject 2. One can see that training errors decrease continuously with epoch number but after about 90th epoch, validation error starts to increase that corresponds to overfitting of classificator. Accordingly, the optimized set of ANN parameters at 90th epoch was used for the estimation of classification accuracy of EEG trials. In this case, the mean accuracy for all 25 subjects was $83.2 \pm 10.8\%$ (mean $\pm$ S.D.) as shown in Fig. 3(c).

The spatiotemporal analysis confirmed our hypothesis that the classification accuracy can be increased by optimizing the number of input channels according to a spatiotemporal structure of the analyzed EEG data. Although significant efforts have been made to disclose the underlying mechanisms for image recognition, the decision-making process in the brain still remains unclear. At least, it is known that perception of ambiguous images engages a distributed neuronal network in parietal, occipital, and frontal lobes.[52,53] Therefore, in this work, we focus on the brain areas involved in the recognition task of the Necker cube orientation interpretation by observing the spatiotemporal distribution of the most discriminative activity. To study the classification accuracy for different EEG channels combination, the training data set was formed for each individual using the first strategy (i) and included 70 EEG trials corresponding to every value of the contrast parameter g. The validation data set also included 70 trials chosen randomly from remaining EEG trials. The number of neurons in the hidden layers was fixed to $H^1 = 19$ and $H^2 = 5$ and the number of the input channels $H^0 = D$ was varied.

The dependencies of the classification accuracy ρ on the network topography of the EEG channels used for ANN training are shown in Fig. 4. One can see that ρ essentially depends on the choice of the EEG channels selected for detection and classification of the brain states. As noted above, the average accuracy using all EEG channels was equal to $83.2 \pm 10.8\%$ [see Figs. 3(b) and 4(a)]. The use of channels from the frontal cortex only ($D = 7$ channels Fp1, Fp2, F3, F4, F7, F8, and Fz) led to a significant decrease in the recognition quality [Fig. 4(b)]. A similar situation was observed when we used EEG channels ($D = 5$ channels T3, C3, Cz, T4, and C4) from the somatosensory cortex [see Fig. 4(c)] and the combination of eight channels ($D = 8$ channels Fp1, Fp2, F7, F8, T3, T4, T5, and T6) from frontal and somatosensory cortex [see Fig. 4(d)]. Obviously, the electrical activity recorded from these spatial areas does not reflect the core features of the spatiotemporal states of the brain dynamics responsible for the interpretation of ambiguous images.

A different situation occurred when we included channels from the occipital region [see Figs. 4(e)–4(h)]. The use of all occipital EEG channels ($D = 8$ channels C3, P3, C4, P4, Cz, Pz, O1, and O2) led to an increase in ρ above 80%, and for some subjects even close to 98% [Fig. 4(e)]. Having compared the mean recognition accuracy obtained for all 25 subjects, one can see that the exclusion of the occipital channels Cz and Pz as well as O1 and O2 led to a significant increase in the averaged classification accuracy to be $74.1 \pm 9.7\%$ [see, e.g., Fig. 4(f)]. Therefore, we suggest that these pairs of EEG channels are crucial for the bistable image interpretation.

To prove this hypothesis, we consider the ANN with only two input signals, either from channels O1 and O2 [Fig. 4(g)] or channels Cz and Pz [Fig. 4(h)]. Figure 3(b) shows the performance of the ANN with only two input signals from channels O1 and O2 (red curves 2) for subject 2. In this case, validation loss starts to grow after 180th epoch that corresponds to overfitting. So, the optimized set of ANN parameters at 180th epoch was used for the estimation of classification accuracy of EEG trials with two O1 and O2 channels. The same results of ANN performance verification are observed for channels Cz and Pz. Using only two occipital channels, the average accuracy was close to $94.4 \pm 10.4\%$ for the pair of O1 and O2, and $95.9 \pm 7.0\%$ for the pair of Cz and Pz, in recognizing different brain states. For some subjects, both pairs of channels gave a high level of recognition accuracy (higher than 95%), while for other subjects, high accuracy was achieved by using only one pair of EEG channels, either O1 and O2 or Cz and Pz. It is worth mentioning that the channels Cz and Pz

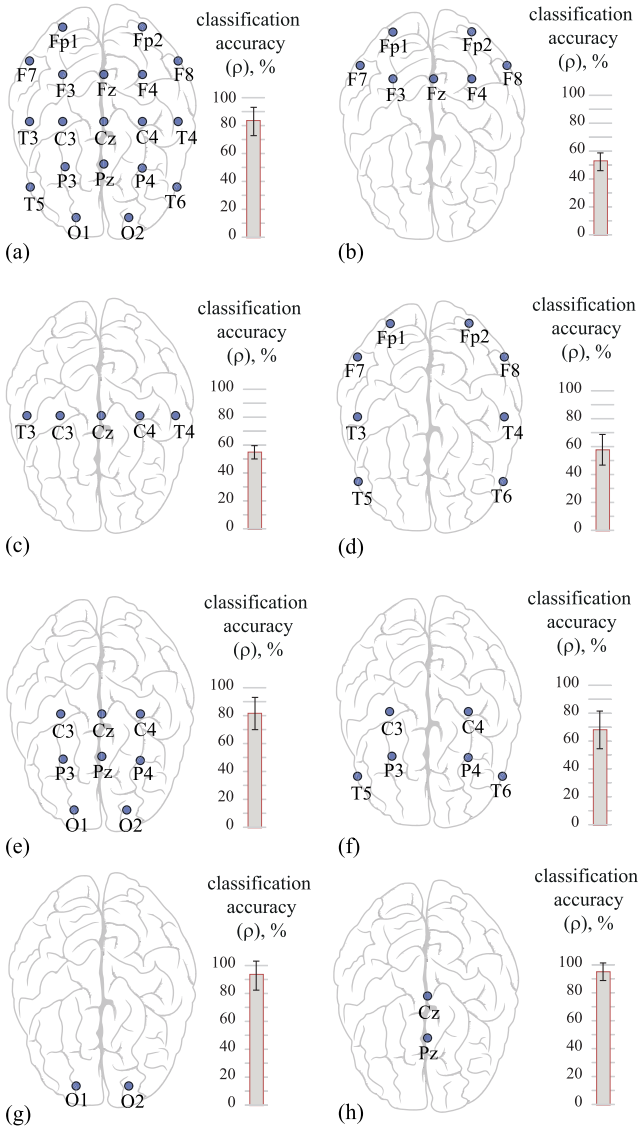

FIG. 4. Classification accuracy for different combinations of input EEG. For each combination, the EEG electrode layout and the classification accuracy averaged over 25 subjects are shown.

demonstrated more stable recognition for all subjects in the group than any other channel pair due to the smaller deviation of the accuracy values. Since the pair Cz and Pz yielded the best recognition results and because we used two channels only that reduced the data processing time, hereinafter we will only consider this pair of EEG channels.

B. Optimal ANN architecture

The choice of the optimal ANN structure is very important issue for classification task. Specifically, if the ANN contains a few number

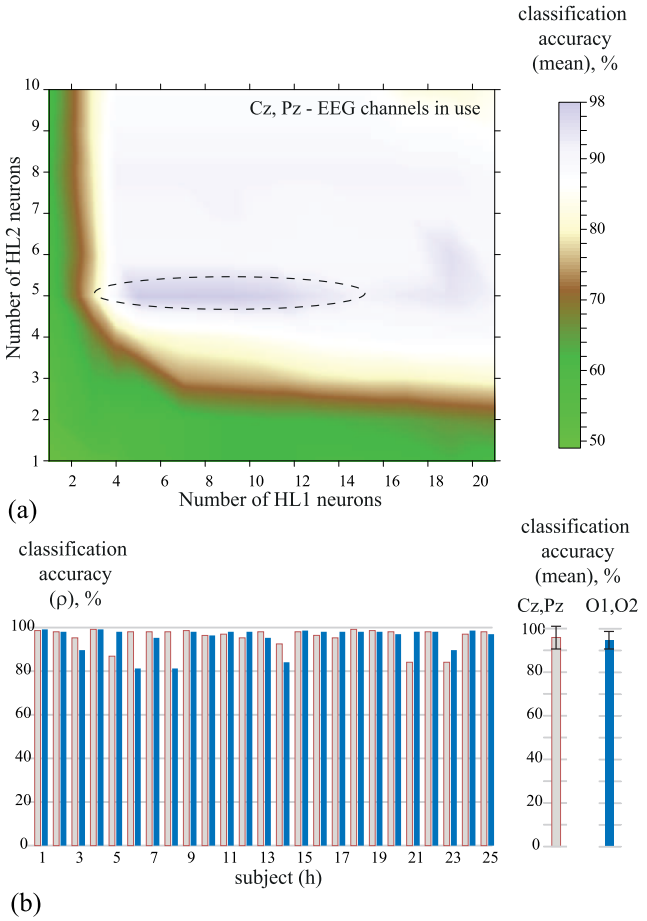

FIG. 5. Classification accuracy for different features of artificial neural network structure in the hidden layers HL1 and HL2. The accuracy ρ was averaged over all 25 subjects. One can see that the averaged accuracy grows rapidly with an increase in the number of neurons in the hidden layers up to $H^1 = H^2 = 5$. One can note that for the chosen ANN parameters ($H_1 > 5$ and $H_2 > 5$), the averaged accuracy ρ exceeded 90%. Obviously, a reasonable compromise between computation simplicity and classification accuracy should be realized.

of neurons in the hidden layers, it cannot provide high classification accuracy. On the other hand, if ANN contains extremely large number of neurons, it takes a very long learning time. Therefore, we must optimize the ANN architecture, i.e., the number of neurons in hidden layers, to get a reasonably accuracy in classification of percept-related EEG trials. In particular, we suggest that the ANN with $H^1 = 19$ neurons is sufficient for the case of only two input EEG channels.

In order to check whether or not the proposed ANN topology is optimal from the viewpoint of event classification using only the Cz and Pz channels, we found how recognition accuracy ρ depended on the numbers H^1 and H^2 of neurons in the hidden layers HL1 and HL2, respectively [Fig. 5(a)]. The accuracy ρ was averaged over all 25 subjects. One can see that the averaged accuracy grows rapidly as the number of neurons in the hidden layers are increased up to 5. Note that for the chosen parameters ($H_1 > 5$

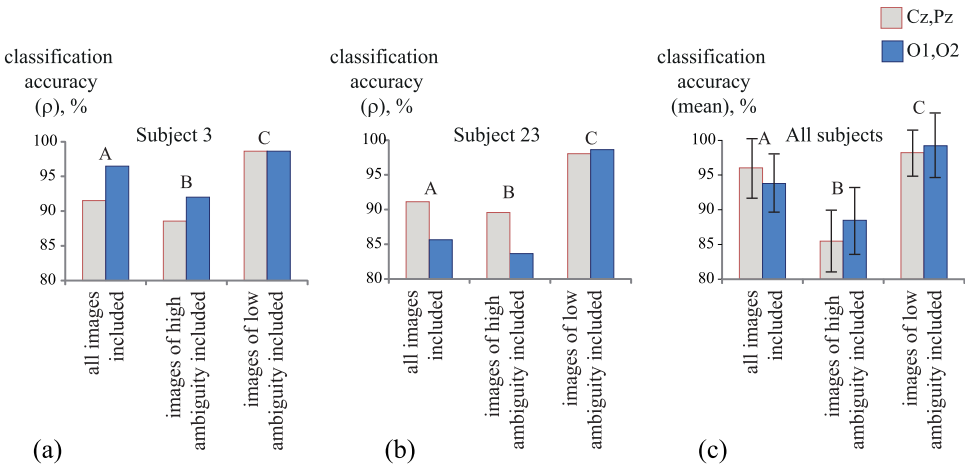

FIG. 6. Classification accuracy for different training set structures. The results are shown for subjects (a) $h = 3$ and (b) $h = 23$ and (c) averaged values over all 25 subjects.

and $H_2 > 5$), the averaged accuracy ρ exceeded 90%. Obviously, a reasonable compromise between the computation simplicity and the classification accuracy should be reached to obtain an optimal ANN architecture. Further, we will use the network architecture with a minimum number of artificial neurons $H^1 = H^2 = 5$ that provide high recognition accuracy. Figure 5(b) illustrates the recognition accuracy of the brain states, using individually trained ANN for each person. We find that the accuracy varied from 82% to 99% with a mean value of 95.7 ± 4.5% for pair (Cz, Pz) and 93.8 ± 4.2% for pair (O1, 02).

C. Selection of images during training to improve classification accuracy

In order to increase classification accuracy, we applied three strategies (ii)–(iv) described above in Sec. III A to check whether or not the training method improved classification performance. In the strategy (ii), the classifier was trained based on randomly chosen $N = 10$ trials, the same for all seven presentations with different contrast parameters regardless of the orientation interpretation (either left- or right-oriented cube for every control parameter g). The strategy (iii) of the training set formation is the selection of trials corresponding to the Necker cubes with high degree of ambiguity (i.e., excluding cubes with low ambiguity $g = 0.15$ and 0.85) regardless of their interpretation. Finally, in the strategy (iv), we formed the training set for the classifier using EEG trials corresponding to the Necker cubes with small degree of ambiguity $g = 0.15$ and 0.85 (i.e., excluding cubes with high ambiguity). The ANN with $H^1 = H^2 = 5$ was then trained with each constructed training set for every subject to determine the recognition accuracy of brain states.

The obtained data for two sample subjects and averaged values over all 25 subjects are shown in Fig. 6 for all considered strategies for the preparation of the training set for both optimal pairs of EEG channels (Cz, Pz and O1, O2). We found that including in the training set the EEG trials corresponding to images with low degree of ambiguity improves the brain state classification performance by approximately 2.8% (varying from 0% to 10.2% for different subjects) for (Cz, Pz) channels and 5.2% (varying from 0% to 14.8% for different subjects) for (O1, O2) channels (cp. cases A and C in Fig. 6). One can see in Fig. 6 (case B) that the exclusion from the training set the trials corresponding to the cubes with low ambiguity led to a drastic decrease in the recognition accuracy by about 10%–15% depending on the choice of EEG channel pairs.

Thus, our experiments showed that the optimal strategy was the classifier trained on the base of the training set composed by EEG trials corresponding to low ambiguous images only ($g = 0.15$ and 0.85). Apparently, human perception of bistable images with low ambiguity exhibited the most pronounced features related to left- or right-oriented cubes recorded by EEG at the occipital lobe.

D. Brain connectivity depending on multistable visual stimulus interpretation

According to neurophysiological brain activity during visual perception, we studied EEG dynamics in five different frequency bands: (i) Δ_δ-range (low-frequency delta 1–4 Hz range), (ii) Δ_θ-range (low-frequency theta 4–7 Hz range), (iii) Δ_α-range (alpha 7–15 Hz range), (iv) Δ_β-range (high-frequency beta 15–30 Hz range), and (v) Δ_γ-range (high-frequency gamma 30–40 Hz range). The wavelet coherence in the ith frequency range Δ_i was calculated as

$$\gamma_{lm}^{\Delta_i} = \frac{1}{f_2 - f_1} \int_{f_1}^{f_2} \gamma_{lm}(f, \Delta\tau)\, df, \tag{11}$$

where f_1 and f_2 are lower and upper boundaries of the considered frequency range. We averaged the values of wavelet coherence $\langle \gamma_{L,ml}^{\Delta_i} \rangle$ and $\langle \gamma_{R,ml}^{\Delta_i} \rangle$ obtained for every pair of EEG channels (l, m) $(l, m = 1, \ldots, P)$ in the ith frequency range over all Necker cube interpretations as left- or right-oriented. Taking into account that EEG channels from the occipital region yielded better recognition results than signals from other regions, we restricted our consideration to the examination of brain connectivity changes in the occipital cortex only.

Figure 7 represents the mean values of the interaction strength $\langle \gamma_{L,ml}^{\Delta_i} \rangle$ between all occipital EEG channels in the different frequency bands Δ^i. We plot only links with strong strengths $\langle \gamma_{L,R}^{\Delta_i} \rangle > 0.8$. The black/red lines between the channels correspond to the brain connectivity in the case of the cube interpretations as left/right-oriented.

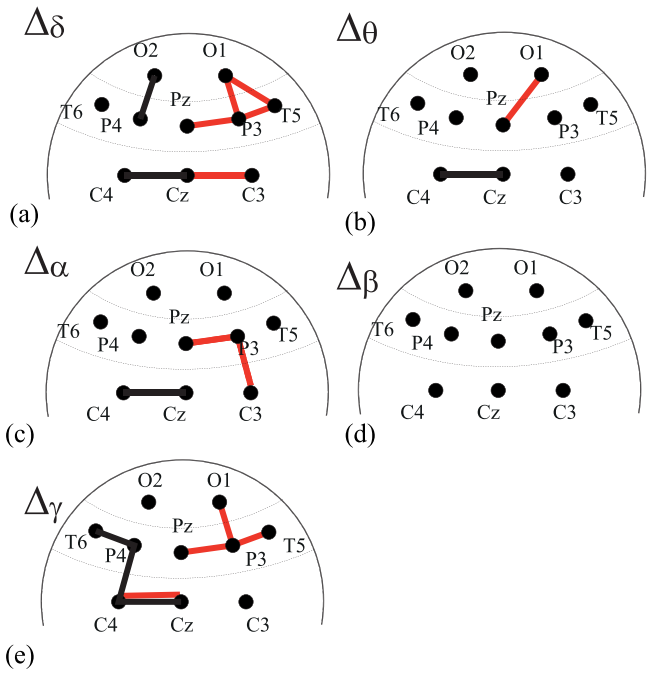

FIG. 7. Schematic illustration of wavelet coherence $\langle \gamma^{\Delta_i}_{L,ml} \rangle$ and $\langle \gamma^{\Delta_i}_{R,ml} \rangle$, reflecting the degree of interaction between different EEG channels from occipital lobe in all considered frequency bands. The shown links have strengths $\langle \gamma^{\Delta_i}_{L,R} \rangle > 0.8$. The black and red lines correspond to left- and right-oriented cube interpretations, respectively.

One can distinguish the difference in the connectivity for different frequency bands. At the same time, there are well-prominent features of occipital cortex connectivity during different Necker cube interpretations: (i) there are no interhemispheric connections, (ii) most of the strong links are connected with Cz and Pz channels in the δ-, θ-, α-, and γ-ranges, while the O1 and O2 channels in the δ-range, and (iii) there is a clearly pronounced asymmetry in the connections for left- and right-oriented cube interpretations.

It should be noted that we did not observe a formation of strong connections in the β-range for both left- and right-oriented cube interpretations. Therefore, we conclude that during ambiguous image interpretation, the brain activity is characterized by a high degree of interaction in all frequency bands (excluding the beta-range) with central nodes in channels Cz and Pz. At the same time, the connections significantly differ for different Necker cube interpretations. In particular, the left-oriented cube interpretation creates connections mainly in the right hemisphere, where the channels Cz and C4 exhibit a strong interaction in all significant frequency ranges, whereas the right-oriented cube perception induces a typical connection between the channels Pz and P3 in the left hemisphere.

The connectivity analysis demonstrated the importance of the channels Cz and Pz, which exhibited a high level of recognition accuracy (more than 95%) of the brain states and more stable recognition results for all the subjects in the analyzed group.

IV. DISCUSSION AND CONCLUSION

Perception and visual information processing are comprehensive actions that involve neural networks in remote brain areas. For instance, the classification of visual stimuli, such as bistable objects, results in complex changes in EEG spectral properties in different brain areas simultaneously. Previous studies of the perception of ambiguous figures using EEG trials, event-related potentials (ERPs) and functional magnetic resonance imaging (fMRI) demonstrated that ambiguous image perception activates and deactivated specific brain areas.[54,55]

At first glance, one expects the perception of visual stimuli to produce the most significant neural activity in the occipital lobe, where the primary visual cortex is located.[56] In particular, according to the ERP analysis, occipital neurons exhibit an increase in the generation of β-waves and a decrease of α-waves.[57] However, the percept-related ERP changes are observed not only in the occipital lobe, but also in the parietal and central lobes.[58]

In general, it was shown that visual perception, along with neuronal activity in the visual cortex, includes poststimulus processes incorporating a re-entrant bias from frontal and parietal areas depending on a particular task.[59,60] This makes it difficult to reduce the number of EEG channels used for the analysis of percept-related EEG, based on the specification of the most relevant brain areas. The more difficult problem is to classify EEG trials associated with different interpretations of an ambiguous visual object. Such a classification task, in turn, is very important for the development of brain-computer interfaces (BCIs), where EEG patterns associated with different interpretations detected in real time can be translated to the corresponding control commands. For the BCI building problem, the reduction of the number of EEG channels is very important, since the setup process with a large number of electrodes is time-consuming and inconvenient for humans. In addition, for real-time application, BCIs with the lowest possible computational complexity are required.

In the present work, we proposed an ANN-based classifier of single EEG traces related to different interpretations of Necker cube images, and optimized the classification algorithm by reducing 90% of the number of the analyzed EEG channels. Our findings show that the highest accuracy (up to 95%) was reached using only two EEG channels for particular sets of EEG channels, namely, for a pair of occipital channels (O1 and O2), and a pair of channels in parietal and central lobe (Cz and Pz).

The significance of such channel combinations is explained by the differences in the structure of brain neuronal network interactions corresponding to different interpretations of the bistable Necker cube. We detected synchronization improvement and, as a consequence, a strong interaction between EEG channels in the occipital lobe after the Necker cube presentation and a further interpretation of its orientation as left- or right-oriented. Then, we analyzed the strength of interaction between all occipital EEG channels for the typical frequency bands: delta, theta, alpha, beta, and gamma. We found that the pair of channels Cz and Pz demonstrated the strongest connections in the δ-, θ-, α-, and γ-ranges, and the pair of channels O1 and O2 in the δ-range.

The set and configuration of connections were significantly different in the case of left- and right-oriented Necker cube interpretations. The left-oriented cube perception was characterized

by connections with the channels Cz and C4 in the right hemisphere in all frequency bands. The right-oriented cube interpretation led to the formation of a connection between the pair of channels Pz and P3 in the left hemisphere. In our opinion, the trained ANN employs features of the EEG signals typical for different cube interpretations and well-pronounced for the most significant pairs of channels (O1, O2) and (Cz, Pz) from the viewpoint of brain connectivity during the Necker cube visual perception.

Interestingly, such a complex cognitive activity can be detected for each single trial based on the consideration of only two EEG channels (which is less than 10% of the available EEG). Earlier studies already revealed the possibility to reduce a number of channels, without a loss of classification/detection task performance by taking a small set of EEG channels ranging from 10 to 30% of available channels. In particular, Chai *et al.*[61] showed that eight channels provided the accuracy rate between 76% and 85% in the classification of a mental task. Moreover, feature reduction approaches, such as a power spectral density and Hilbert-Huang transform, allowed them to reach the accuracy rate between 70% and 84% using two channels only. Next, for the classification of motor-related EEG, Wang *et al.*[62] used four channels, which allowed them to get the average accuracy rate of up to 92.66%, whereas the use of eight channels provided 94.96% accuracy. They performed the channel reduction by a common spatial pattern method. Later, Piryatinska *et al.*[63] demonstrated 87.41% and 87.2% accuracy in classification of sleep stages basing on four and five channels, respectively.

Impressively, the classification accuracy for the selected channels can be higher than when using all channels (95% vs 85%). Such an effect was previously observed in the classification of EEG trials associated with epileptic seizures[64] and imaginary movements.[65] This means that in some cases, the use of too many channels not only overloads the computational cost, but also leads to worsening classification accuracy due to increasing data complexity.[66]

It is important to note that in our study the optimization was based on the EEG properties revealed from the analysis of the group of 25 participants. This makes our results general because of low intersubject variability. In this respect, other optimization approaches, such as wrapper or filtering techniques, which searched for the optimal EEG channel combination by analyzing the data of each subject, and therefore the optimal channel combination varied very much from subject to subject.

In conclusion, this paper is devoted to ML methods application to detect and classify EEG patterns corresponding to visual perception. By optimizing the artificial neuronal network architecture for obtained experimental multichannel EEG data, we have developed the automatic system for the recognition of the EEG patterns associated with two possible decisions about the ambiguous Necker cube orientation (either left- or right-oriented) and obtained about 95% accuracy using only a pair of EEG channels at the occipital region (locations O1, O2 or Cz, Pz of the typical "10—20" EEG registration scheme). These spatial features of the EEG data set have been observed for all experiments with the different subjects so that the ANN, trained with only two channels in the brain occipital area, was able to classify the corresponding brain states with very high accuracy. We have described an optimal strategy to construct training EEG trial data sets for optimal ANN learning. It should be emphasized that our results do not depend on motor activity (real or imaginary), because to exclude motor activity effects, we have carried out an additional experiment with key pressing.

The significance of the our experimental and numerical results is not limited to the brain processing of ambiguous figures, such as a considered here bistable perception cube, but can also be extended to the recognition of brain states associated with different decisions while performing complex tasks. The conducted experiments and developed artificial intelligence classification method will be useful for analyzing and recognizing different brain states using neurophysiological multichannel signals and can stimulate future studies in the field of experimental and computational neuroscience. In particular, it allows the identification of the most important brain areas for the classification of neuronal activity, as well as highlight the most significant types of stimuli. We are sure that the developed optimization approach of ML systems to quantitatively characterize brain activity can be used in neurotechnology, e.g., for designing brain-computer interfaces[67,68] for rehabilitation[69,70] and diagnostic and prognostic purposes.[71,72] The robustness of brain-computer interfaces (BCIs) is defined by the neurointerface operator's ability to generate the same EEG responses to the same stimuli, i.e., BCI is affected by intersubject variability.[73] In this respect, our results open the possibility to develop a unified ANN-based classifier. This in turn provides promising conditions for creating BCIs, suitable for multiple and untrained users.[74,75] The obtained results will be useful for researchers working in interdisciplinary areas at the cutting edge of engineering, mathematics, nonlinear dynamics, neuroscience, and medicine.

ACKNOWLEDGMENTS

The work has been supported by the Russian Science Foundation (Grant No. 17-72-30003).

REFERENCES

[1] B. Lusch, J. N. Kutz, and S. L. Brunton, "Deep learning for universal linear embeddings of nonlinear dynamics," Nat. Commun. **9**, 4950 (2018).
[2] T. Weng, H. Yang, C. Gu, J. Zhang, and M. Small, "Synchronization of chaotic systems and their machine-learning models," Phys. Rev. E **99**, 042203 (2019).
[3] J. Pathak, Z. Lu, B. R. Hunt, M. Girvan, and E. Ott, "Using machine learning to replicate chaotic attractors and calculate Lyapunov exponents from data," Chaos **27**, 121102 (2017).
[4] Z. Lu, B. R. Hunt, and E. Ott, "Attractor reconstruction by machine learning," Chaos **28**, 061104 (2018).
[5] D. Ibáñez-Soria, J. Garcia-Ojalvo, A. Soria-Frisch, and G. Ruffini, "Detection of generalized synchronization using echo state networks," Chaos **28**, 033118 (2018).
[6] Y. Ma, X. Ding, Q. She, Z. Luo, T. Potter, and Y. Zhang, "Classification of motor imagery EEG signals with support vector machines and particle swarm optimization," Comput. Math. Methods Med. **2016**, 4941235.
[7] A. W. L. Chiu, S. S. Jahromi, H. Khosravani, P. L. Carlen, and B. L. Bardakjian, "The effects of high-frequency oscillations in hippocampal electrical activities on the classification of epileptiform events using artificial neural networks," J. Neural Eng. **3**, 9 (2006).
[8] A. E. Hramov, N. S. Frolov, V. A. Maksimenko, V. V. Makarov, A. A. Koronovskii, J. Garcia-Prieto, L. F. Antón-Toro, F. Maestú, and A. N. Pisarchik, "Artificial neural network detects human uncertainty," Chaos **28**, 033607 (2018).
[9] M. Hajinoroozi, Z. Mao, T.-P. Jung, C.-T. Lin, and Y. Huang, "EEG-based prediction of driver's cognitive performance by deep convolutional neural network," Signal Process. Image Commun. **47**, 549–555 (2016).
[10] V. A. Maksimenko, S. A. Kurkin, E. N. Pitsik, V. Y. Musatov, A. E. Runnova, T. Y. Efremova, A. E. Hramov, and A. N. Pisarchik, "Artificial neural network

classification of motor-related EEG: An increase in classification accuracy by reducing signal complexity," Complexity **2018**, 9385947 (2018).
[11] A. E. Hramov, V. A. Maksimenko, S. V. Pchelintseva, A. E. Runnova, V. V. Grubov, V. Y. Musatov, M. O. Zhuravlev, A. A. Koronovskii, and A. N. Pisarchik, "Classifying the perceptual interpretations of a bistable image using EEG and artificial neural networks," Front. Neurosci. **11**, 674 (2017).
[12] E. S. Nurse, P. J. Karoly, D. B. Grayden, and D. R. Freestone, "A generalizable brain-computer interface (BCI) using machine learning for feature discovery," PLoS One **10**, 0131328 (2015).
[13] K. Bowsher, E. F. Civillico, J. Coburn, J. Collinger, J. L. Contreras-Vidal, T. Denison, J. Donoghue, J. French, N. Getzoff, L. R. Hochberg, M. Hoffmann, J. Judy, N. Kleitman, G. Knaack, V. Krauthamer, K. Ludwig, M. Moynahan, J. J. Pancrazio, P. H. Peckham, C. Pena, V. Pinto, T. Ryan, D. Saha, H. Scharen, S. Shermer, K. Skodacek, P. Takmakov, D. Tyler, S. Vasudevan, K. Wachrathit, D. Weber, C. G. Welle, and M. Ye, "Brain-computer interface devices for patients with paralysis and amputation: A meeting report," J. Neural Eng. **13**, 023001 (2016).
[14] L. R. Quitadamo, F. Cavrini, L. Sbernini, F. Riillo, L. Bianchi, S. Seri, and G. Saggio, "Support vector machines to detect physiological patterns for EEG and EMG-based human-computer interaction: A review," J. Neural Eng. **14**, 011001 (2017).
[15] M. C. Åberg and J. Wessberg, "Evolutionary optimization of classifiers and features for single-trial EEG discrimination," Biomed. Eng. Online **6**, 32–32 (2007).
[16] F. G. Alpert, R. Manor, A. B. Spanier, L. Y. Deouell, and A. B. Geva, "Spatiotemporal representations of rapid visual target detection: A single-trial EEG classification algorithm," IEEE Trans. Biomed. Eng. **61**, 2290–2303 (2014).
[17] J. C. G. D. Costa, P. J. G. Da-Silva, R. M. V. R. Almeida, and A. F. C. Infantosi, "Validation in principal components analysis applied to EEG data," Comput. Math. Methods Med. **2014**, 413801.
[18] A. A. Putilov, "Principal component analysis of the EEG spectrum can provide yes-or-no criteria for demarcation of boundaries between NREM sleep stages," Sleep Sci. **8**, 16–23 (2015).
[19] R. Zhang, P. Xu, L. Guo, Y. Zhang, P. Li, and D. Yao, "Z-score linear discriminant analysis for EEG based brain-computer interfaces," PLoS One **8**, e74433 (2013).
[20] E. Neto, F. Biessmann, H. Aurlien, H. Nordby, and T. Eichele, "Regularized linear discriminant analysis of EEG features in dementia patients," Front. Aging Neurosci. **8**, 273 (2016).
[21] H. Li, D. Yuan, X. Ma, D. Cui, and L. Cao, "Genetic algorithm for the optimization of features and neural networks in ECG signals classification," Sci. Rep. **7**, 41011 (2017).
[22] J. Yang, H. Singh, E. L. Hines, F. Schlaghecken, D. D. Iliescu, M. S. Leeson, and N. G. Stocks, "Channel selection and classification of electroencephalogram signals: An artificial neural network and genetic algorithm-based approach," Artif. Intell. Med. **55**, 117–126 (2012).
[23] S. B. Nanthini and B. Santhi, "Electroencephalogram signal classification for automated epileptic seizure detection using genetic algorithm," J. Nat. Sci. Biol. Med. **8**, 159–166 (2017).
[24] S. Smith, "Linking cognition to brain connectivity," Nat. Neurosci. **19**, 7 (2016).
[25] J. Kornmeier, E. Friedel, M. Wittmann, and H. Atmanspacher, "EEG correlates of cognitive time scales in the Necker-Zeno model for bistable perception," Conscious. Cogn. **53**, 136–150 (2017).
[26] P. Chholak, G. Niso, V. A. Maksimenko, S. A. Kurkin, N. S. Frolov, E. N. Pitsik, A. E. Hramov, and A. N. Pisarchik, "Visual and kinesthetic modes affect motor imagery classification in untrained subjects," Sci. Rep. **9**, 9838 (2019).
[27] World Medical Association, "World Medical Association (2000) Declaration of Helsinki: Ethical principles for medical research involving human subjects," J. Am. Med. Assoc. **284**, 3043–3045 (2000).
[28] L. A. Necker, "Observations on some remarkable phenomena seen in Switzerland; and an optical phenomenon which occurs on viewing of a crystal or geometrical solid," Philos. Mag. **3**, 329–343 (1832).
[29] A. N. Pisarchik, R. Jaimes-Reategui, C. D. A. Magallón-Garcia, and C. O. Castillo-Morales, "Critical slowing down and noise-induced intermittency in bistable perception: Bifurcation analysis," Biol. Cybern. **108**, 397–404 (2014).
[30] A. Pastukhov, P. E. García-Rodriguez, J. Haenicke, A. Guillamon, G. Deco, and J. Braun, "Multi-stable perception balances stability and sensitivity," Front. Comput. Neurosci. **7**, 17 (2013).
[31] R. H. S. Carpenter, "Analysing the detail of saccadic reaction time distributions," Biocybern. Biomed. Eng. **32**, 49–63 (2012).
[32] I. Merk and J. Schnakenberg, "A stochastic model of multistable visual perception," Biol. Cybern. **86**, 111–116 (2002).
[33] D. A. Leopold, M. Wilke, A. Maier, and N. K. Logothetis, "Stable perception of visually ambiguous patterns," Nat. Neurosci. **5**, 605–609 (2002).
[34] J. Kornmeier, W. Ehn, H. Bigalke, and M. Bach, "Discontinuous presentation of ambiguous figures: How interstimulus-interval durations affect reversal dynamics and ERPs," Psychophysiology **44**, 552 (2007).
[35] E. Niedermeyer and F. L. da Silva, *Electroencephalography: Basic Principles, Clinical Applications, and Related Fields* (Lippincot Williams & Wilkins, 2004).
[36] S. Haykin, *Neural Networks: A Comprehensive Foundation*, 3rd ed. (Pearson, 2008).
[37] R. Duda and P. Hart, *Pattern Classification and Scene Analysis* (Wiley, New York, 1973).
[38] E. Haselsteiner and G. Pfutscheller, "Using time-dependent neural networks for EEG classification," IEEE Trans. Rehabil. Eng. **8**, 457–463 (2000).
[39] C. L. Fontoura da and J. R. M. Cesar, *Shape Analysis and Classification: Theory and Practice* (CRC Press, Boca Raton, FL, 2001).
[40] D. Garrett, D. A. Peterson, C. W. Anderson, and M. H. Thaut, "Comparison of linear, nonlinear, and feature selection methods for EEG signal classification," IEEE Trans. Neural Syst. Rehabil. Eng. **11**, 141–144 (2003).
[41] N. S. Dias, M. Kamrunnahar, P. M. Mendes, S. J. Schiff, and J. H. Correia, "Comparison of EEG pattern classification methods for brain-computer interfaces," Conf. Proc. IEEE Eng. Med. Biol. Soc. **2007**, 2540 (2007).
[42] M. R. Hasan, M. I. Ibrahimy, S. M. Motakabber, and S. Shahid, *Classification of Multichannel EEG Signal by Linear Discriminant Analysis* (Springer International Publishing, 2015), Chap. 0, 279–282.
[43] X. Yao, "Evolving artificial neural networks," Proc. IEEE **87**, 1423–1447 (1999).
[44] G. Cybenko, "Approximation by superpositions of a sigmoidal function," in *Mathematics of Control, Signals, and Systems* (Springer International, 2006), pp. 303–314.
[45] T. Strutz, *Data Fitting and Uncertainty (A Practical Introduction to Weighted Least Squares and Beyond)*, 2nd ed. (Springer, 2016).
[46] B. Torresani, *Continuous Wavelet Transform* (Savoire, Paris, 1995).
[47] A. N. Pavlov, A. E. Hramov, A. A. Koronovskii, Y. E. Sitnikova, V. A. Makarov, and A. A. Ovchinnikov, "Wavelet analysis in neurodynamics," Phys-Usp+ **55**, 845–875 (2012).
[48] V. A. Maksimenko, A. Luttjohann, V. V. Makarov, M. V. Goremyko, A. A. Koronovskii, V. O. Nedaivozov, A. E. Runnova, G. Van Luijtelaar, A. E. Hramov, and S. Boccaletti, "Macroscopic and microscopic spectral properties of brain networks during local and global synchronization," Phys. Rev. E **96**, 012316 (2017).
[49] V. V. Makarov, M. O. Zhuravlev, A. E. Runnova, P. Protasov, V. A. Maksimenko, N. S. Frolov, A. N. Pisarchik, and A. E. Hramov, "Betweenness centrality in multiplex brain network during mental task evaluation," Phys. Rev. E **98**, 062413 (2018).
[50] A. E. Hramov, A. A. Koronovskii, V. A. Makarov, A. N. Pavlov, and E. Sitnikova, *Wavelets in Neuroscience*, Springer Series in Synergetics (Springer, Heidelberg, 2015).
[51] V. A. Maksimenko, A. E. Runnova, N. S. Frolov, V. V. Makarov, V. Nedaivozov, A. A. Koronovskii, A. Pisarchik, and A. E. Hramov, "Multiscale neural connectivity during human sensory processing in the brain," Phys. Rev. E **97**, 052405 (2018).
[52] F. Tong, M. Meng, and R. Blake, "Neural bases of binocular rivalry," Trends Cogn. Sci. (Regul. Ed.) **10**, 502–511 (2006).
[53] P. Sterzer, A. Kleinschmidt, and G. Rees, "The neural bases of multistable perception," Trends Cogn. Sci. (Regul. Ed.) **13**, 310–318 (2009).
[54] T. Inui, S. Tanaka, T. Okada, S. Nishizawa, M. Katayama, and J. Konishi, "Neural substrates for depth perception of the Necker cube; a functional magnetic resonance imaging study in human subjects," Neurosci. Lett. **282**, 145 (2000).
[55] T. J. Müller, A. Federspiel, H. Horn, K. Lovblad, C. Lehmann, T. Dierks, and W. Strick, "The neurophysiological time pattern of illusionary visual perceptual

transitions: A simultaneous EEG and fMRI study," Int. J. Psychophysiol. **55**, 299 (2005).
[56]R. Desimone and J. Duncan, "Neural mechanisms of selective visual attention," Annu. Rev. Neurosci. **18**, 193–222 (1995).
[57]T. Ergenoglu, T. Demiralp, Z. Bayraktaroglu, M. Ergen, H. Beydagi, and Y. Uresin, "Alpha rhythm of the EEG modulates visual detection performance in humans," Cogn. Brain Res. **20**, 376–383 (2004).
[58]P. C. J. Taylor and G. Thut, "Brain activity underlying visual perception and attention as inferred from TMS–EEG: A review," Brain Stimul. **5**, 124–129 (2012).
[59]A. C. Nobre, "The attentive homunculus: Now you see it, now you don't," Neurosci. Biobehav. Rev. **25**, 477–496 (2001).
[60]M. Corbetta and G. L. Shulman, "Control of goal-directed and stimulus-driven attention in the brain," Nat. Rev. Neurosci. **3**, 201 (2002).
[61]R. Chai, S. H. Ling, G. P. Hunter, and H. T. Nguyen, "Toward fewer EEG channels and better feature extractor of non-motor imagery mental tasks classification for a wheelchair thought controller," in *2012 Annual International Conference of the IEEE Engineering in Medicine and Biology Society* (IEEE, 2012), pp. 5266–5269.
[62]Y. Wang, S. Gao, and X. Gao, "Common spatial pattern method for channel selection in motor imagery based brain-computer interface," in *27th Annual International Conference of the IEEE Engineering in Medicine and Biology Society (IEEE-EMBS), 2005* (IEEE, 2006), pp. 5392–5395.
[63]A. Piryatinska, W. A. Woyczynski, M. S. Scher, and K. A. Loparo, "Optimal channel selection for analysis of EEG-sleep patterns of neonates," Comput. Methods Programs Biomed. **106**, 14–26 (2012).
[64]B. R. Greene, G. B. Boylan, W. P. Marnane, G. Lightbody, and S. Connolly, "Automated single channel seizure detection in the neonate," in *2008 30th Annual International Conference of the IEEE Engineering in Medicine and Biology Society* (IEEE, 2008), pp. 915–918.
[65]M. Li, J. Ma, and S. Jia, "Optimal combination of channels selection based on common spatial pattern algorithm," in *2011 IEEE International Conference on Mechatronics and Automation* (IEEE, 2011), pp. 295–300.
[66]T. N. Lal, M. Schroder, T. Hinterberger, J. Weston, M. Bogdan, N. Birbaumer, and B. Scholkopf, "Support vector channel selection in BCI," IEEE Trans. Biomed. Eng. **51**, 1003–1010 (2004).
[67]C. J. Bell, P. Shenoy, R. Chalodhorn, and R. Rao, "Control of a humanoid robot by a noninvasive brain computer interface in humans," J. Neural Eng. **5**, 214 (2008).
[68]D. J. McFarland, M. A. Parvaz, W. A. Sarnacki, R. Z. Goldstein, and J. R. Wolpaw, "Prediction of subjective ratings of emotional pictures by EEG features," J. Neural Eng. **14**, 016009 (2017).
[69]E. Yom-Tov and G. F. Inbar, "Feature selection for the classification of movements from single movement-related potentials," IEEE Trans. Neural Syst. Rehabil. Eng. **10**, 170–177 (2002).
[70]K. K. Ang, K. S. G. Chua, K. S. Phua, C. Wang, Z. Y. Chin, C. W. K. Kuah, W. Low, and C. Guan, "A randomized controlled trial of EEG-based motor imagery brain-computer interface robotic rehabilitation for stroke," Clin. EEG Neurosci. **46**, 310–320 (2015).
[71]A. A. Ovchinnikov, A. Luttjohann, A. E. Hramov, and G. van Luijtelaar, "An algorithm for real-time detection of spike-wave discharges in rodents," J. Neurosci. Methods **194**, 172–178 (2010).
[72]V. A. Maksimenko, S. Heukelum van, V. V. Makarov, J. Kelderhuis, A. Luttjohann, A. A. Koronovskii, A. E. Hramov, and G. Luijtelaar van, "Absence seizure control by a brain computer interface," Sci. Rep. **7**, 2487 (2017).
[73]A. Ferrante, C. Gavriel, and A. Faisal, "Data-efficient hand motor imagery decoding in EEG-BCI by using Morlet wavelets & common spatial pattern algorithms," in *7th International IEEE/EMBS Conference on Neural Engineering (NER)* (IEEE, 2015), p. 948.
[74]B. Blankertz, G. Dornhege, M. Krauledat, K. R. Muller, and G. Curio, "The non-invasive Berlin brain-computer interface: Fast acquisition of effective performance in untrained subjects," NeuroImage **37**, 539 (2007).
[75]K. R. Müler, M. Tangermann, G. Dornhege, M. Krauledat, G. Curio, and B. Blankertz, "Machine learning for real-time single-trial EEG-analysis: From brain-computer interfacing to mental state monitoring," J. Neurosci. Methods **167**, 82–90 (2008).